Journal of Earth Science, *Vol. 21*, *No. 5*, *p. 792–800*, *October 2010* *ISSN 1674-487X*
Printed in China
DOI: 10.1007/s12583-010-0115-z

Acoustic Velocities and Elastic Properties of Pyrite (FeS_2) to 9.6 GPa

Matthew L Whitaker*
Mineral Physics Institute, *Stony Brook University*, *New York* 11794-2100, *USA*; *Geodynamics Research Center*, *Ehime University*, *Matsuyama* 790-8577, *Japan*
Wei Liu, **Liping Wang**, **Baosheng Li**
Mineral Physics Institute, *Stony Brook University*, *New York* 11794-2100, *USA*

ABSTRACT: Ultrasonic interferometry was utilized in conjunction with synchrotron-based X-ray diffraction and X-radiographic imaging to determine the compressional and shear wave velocities and unit-cell volumes of pyrite (FeS_2) at room temperature and pressures up to 9.6 GPa. Fitting all of the experimental volume and velocity data to third-order finite-strain equations yielded the adiabatic zero-pressure bulk and shear moduli and their first pressure derivatives: K_{S0}=138.9(7) GPa, G_0=112.3(3) GPa, $(\partial K_{S0}/\partial P)_T=K_{S0}'$=6.0(1), $(\partial G_0/\partial P)_T=G_0'$=3.0(<1), where the numbers in parentheses represent the 1σ uncertainty in the last significant digit. These results are in good agreement with several previous static compression studies on this material but differ quite strongly from the results obtained via first principles calculations. This study presents the first direct measurement of the bulk shear properties of this material.

KEY WORDS: mineral physics, ultrasonic interferometry, high pressure, iron sulfide, elastic property, equation of state.

INTRODUCTION

The composition of the earth's core has been a long standing question in the field of the earth sciences (e.g., McDonough and Sun, 1995) since its discovery over a century ago (Oldham, 1906). Our ability to determine the structure and composition of the deep interior of the earth is limited because we lack the capability of direct observation. Therefore, we have to rely on the tools we have available, most notably seismology and mineral physics, and to make interpretations about what is present in the deep earth interior. Compilation and analysis of a large population of seismic data gave rise to the Preliminary Reference Earth Model (PREM) of Dziewonski and Anderson (1981). While seismic models give us information on the density and velocity structure of the earth's interior, they do not give any compositional information. In order to determine what the composition of the various regions of the earth's interior may be, the physical properties of candidate deep earth materials under conditions of high pressure and high

This study was supported by the USA National Science Foundation (Nos. EAR00135550, EAR0635860) to Baosheng Li, the USA Department of Energy, Office of Science, Office of Basic Energy Sciences (No. DE-AC02-98CH10886), the Consortium for Materials Properties Research in Earth Sciences under NSF Cooperative Agreement (No. EAR01-35554), and the Mineral Physics Institute, Stony Brook University (MPI Publication No. 480).

*Corresponding author: matt@mattwhitaker.net

© China University of Geosciences and Springer-Verlag Berlin Heidelberg 2010

Manuscript received May 4, 2010.
Manuscript accepted June 7, 2010.

temperature must be investigated, and then, these data obtained via mineral physics studies must be compared to the seismic profiles of the earth's interior, such as PREM.

It has long been accepted that the core of the earth, as well as those of other terrestrial planetary bodies, is predominantly made up of metallic iron or an iron-nickel alloy (e.g., Jeanloz, 1990), though studies have shown that metallic Fe alone is too dense to be the sole element in the earth's core; particularly, the solid inner core (e.g., Mao et al., 1998; Jephcoat and Olson, 1987). These studies and others suggest that there must be some amount of one or more light elements in the core. In order to assess which elements might be present within the core of the earth, and in what possible proportions, the physical properties of various iron/light-element alloys (ILEAs) under extreme conditions must be ascertained and compared against the information gained from seismic studies of the earth's interior.

Sulfur has been extensively investigated as a possible core constituent and has been met with mixed results; element partitioning seems to suggest that S is the most likely light element to be incorporated into the core during its formation (e.g., Li and Agee, 2001). Experimental studies have indicated that the presence of a significant amount of S in the core is unlikely with respect to other possible light elements (e.g., Badro et al., 2007), while other experiments have suggested that the earth's inner core does contain a significant amount of S (e.g., Li et al., 2001). Previous work has also suggested that the deviations in density and seismic velocities from pure iron observed in the inner core can be accounted for by having S present in the inner core in addition to another light element (Dreibus and Palme, 1996).

This study was designed to determine the physical properties of pyrite (FeS_2) under extreme conditions in order to expand our understanding of this material and help to place constraints on the possible light element content of the earth's core. Pyritic FeS_2 occurs in a cubic structure in space group *Pa*3 at room temperature and pressure (Merkel et al., 2002). Previous studies have characterized the many differences between samples and examined the thermal expansion of pyrite (Chrystall, 1965; Smith, 1942), and there have been several experimental and computational studies conducted at high pressure (both static and dynamic) to determine the Raman spectra, electronic structure, elasticity, and equation-of-state of pyrite (Blanchard et al., 2005; Le Page and Rodgers, 2005; Kleppe and Jephcoat, 2004; Sithole et al., 2003; Merkel et al., 2002; Ahrens and Jeanloz, 1987; Fujii et al., 1986; Chattopadhyay and von Schnering, 1985; Drickamer et al., 1967). In addition, studies have determined the single-crystal elastic constants of pyrite (Benbattouche et al., 1989; Simmons and Birch, 1963; Prasad and Wooster, 1956).

As is the case for many other ILEAs (see Whitaker et al., 2009, 2008), the results of previous studies on pyrite contain a great deal of inconsistency. In addition, there has not yet been any high-pressure (>0.15 GPa) data made available on the elastic shear properties of pyrite. In order to fill this void in the experimental literature and attempt to solve the controversy regarding the physical properties of this material, we studied a sample of pyrite in situ at high pressure using a combination of synchrotron-based X-ray diffraction, X-radiographic imaging, and ultrasonic interferometry in a large volume multi-anvil cell (MAC).

METHODS

The pyrite starting material used in this work was purchased from Alfa Aesar in powdered form (99.9% pure) packed under an argon atmosphere. This powder was significantly hygroscopic and tended to react with moisture and oxygen from the air to form sulfate; as such, the material was kept in a desiccator at all times when not actively being used. The powder was hand ground for more than 30 min in an agate mortar, resulting in a fine powder with an average grain size on the order of a few microns. X-ray powder diffraction on this fine powder confirmed that the starting material was pure homogeneous pyrite.

This fine powder was tightly packed into an Au capsule and dried overnight at 150 ℃ to drive off any adsorbed moisture; after which, the capsule was pressure sealed to prevent any readsorption of moisture. This sample was then sintered at 10 GPa and 900 ℃ for 1 h using a standard 14/8 octahedral cell assembly in a 2 000-t uniaxial split-cylinder apparatus at Stony

Brook University's High Pressure Laboratory, after which it was quenched to room temperature and decompressed over 18 h. The density of the recovered sample was measured via the Archimedes method and was found to be 99.2% of the theoretical density. Figure 1 shows an SEM image of the unpolished sample. There appears to be a bimodal grain size distribution, with the larger grains averaging 2–3 μm, and the smaller averaging around half a micron; triple junctions can be seen in several grain boundaries in this image, indicating low porosity and a good sintering. The EDS spectra collected in several areas were identical to each other, and there was no evidence of any impurities. X-ray diffraction of both the surface and interior of the sintered cylinder indicated that the sample was pure homogeneous pyrite; no oxidation of the sample was detected via either SEM (scanning electron microscope) or XRD (X-ray diffraction).

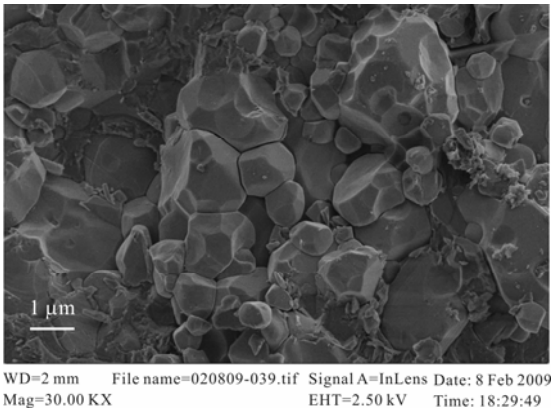

Figure 1. SEM image of the rough and unpolished surface of the pyrite (FeS_2) sample used in this study.

The in situ synchrotron-based ultrasonic experiment was conducted in the cubic-anvil apparatus (SAM85) installed at beamline X17B2 of the National Synchrotron Light Source (NSLS). A detailed description and schematic diagram of the experimental setup can be found in Whitaker et al. (2008). To ensure a minimal loss of acoustic energy during the ultrasonic measurements, all surfaces along the acoustic travel path (both sides of the sample, buffer rod, and WC anvil on which the transducer was mounted) were polished with 1 μm diamond paste to be perfectly flat and parallel within 0.05º. The sample, surrounded by a pseudohydrostatic environment consisting of a BN sleeve and a 10 : 1, NaCl : BN mixture, was slowly brought up to the maximum load of 60 t at room temperature, stopping every six tons along the way to collect ultrasonic data, an X-radiographic image, and an X-ray diffraction pattern of the sample and the NaCl pressure marker. After the data at the peak pressure were collected, the heating of the sample resulted in a catastrophic blowout of the anvils in the press, destroying the sample and ending the experiment. Thus, no data could be collected at high temperature or during decompression.

Ultrasonic interferometry measurements were made using a dual mode $LiNbO_3$ transducer (10º Y-cut) capable of producing and receiving acoustic waves with frequencies ranging from 20–70 MHz, allowing for simultaneous determination of P- and S-wave travel times with standard deviations of ~0.2 and ~0.4 ns, respectively. The transfer function method (Li et al., 2002) was used to record the acoustic response of the cell assembly over the above frequency range, after which the monochromatic waveform data were extracted for P- (55 MHz) and S-waves (35 MHz), and the pulse echo overlap technique was used to obtain the two-way travel times of these waves through the sample. More information on processing the data from these measurements can be found elsewhere (Li et al., 2004, 2002).

Energy dispersive X-ray diffraction patterns were collected using a solid-state Ge detector with the incident white X-ray beam collimated to 100×100 μm. The 2θ angle was calibrated at 6.693º for this experiment. X-ray diffraction was collected for 120 s on the NaCl standard and for 180 s on the pyrite sample. X-radiographic images of the sample region were recorded using a CCD camera, and these images gave a precise measure of the length of the sample. A pixel-to-length ratio was determined using the measured sample length and the image length of the sample at ambient pressure, and this ratio was applied to every image collected, thereby yielding the absolute length of the sample as a function of pressure with a precision of ~0.2%–0.4% (Li et al., 2004). From sample lengths and travel times, P- and S-wave velocities are directly obtained, and the density of the material is obtained via cell refinement of the sample X-ray diffraction pattern. The density and acoustic velocities

give a direct measurement of the shear ($G=\rho V_S^2$) and adiabatic bulk ($K_S=\rho V_P^2-4G/3$) moduli at each pressure explored.

RESULTS

All of the experimental data for this experiment are given in Table 1. The X-ray diffraction patterns collected indicated that pyrite does not undergo any phase transitions in the pressure range explored (Fig. 2). This is consistent with the results of all previous studies on this material (Blanchard et al., 2005; Le Page and Rodgers, 2005; Sithole et al., 2003; Merkel et al., 2002; Benbattouche et al., 1989; Ahrens and Jeanloz, 1987; Fujii et al., 1986; Chattopadhyay and von Schnering, 1985; Drickamer et al., 1967; Simmons and Birch, 1963; Prasad and Wooster, 1956; Bridgman, 1949). Depending on the pressure and interference from Pb fluorescence peaks arising from the extensive lead shielding in the experimental hutch, a total of 12–15 diffraction lines were used in the refinement to determine the unit-cell volume of FeS_2, with a relative standard deviation less than 0.05%. X-ray diffraction patterns of the sample indicate no discernable increase in the X-ray diffraction peak widths (FWHM), which implies a low deviatoric stress level on the sample.

The unit-cell volumes obtained from the refinements (using the space group *Pa*3) exhibit a smooth trend of decreasing volume with increasing pressure (Fig. 3). A value of 159.01(3) $Å^3$ was obtained for the unit-cell volume at ambient conditions (V_0), which is

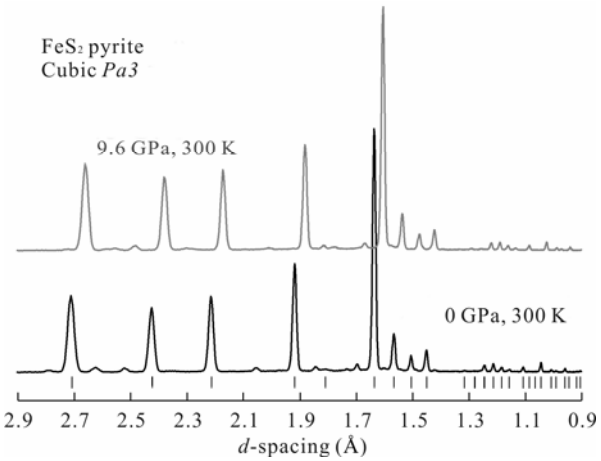

Figure 2. X-ray diffraction patterns of FeS_2 sample at 0 and 9.6 GPa. Vertical lines below diffraction pattern indicate peak positions in the standard powder diffraction file that were used to index the pattern. Unmarked peaks are the result of parasitic scattering from the surrounding material in the cell assembly.

Table 1 Experimental ultrasonic and X-ray results on FeS_2 at room temperature

P^a (GPa)	P^b (GPa)	ρ (g·cm^{-3})	2*tp* (μs)	2*ts* (μs)	*L* (mm)	*V* (Å^3)	V_P (km·s^{-1})	V_S (km·s^{-1})	K_S (GPa)	*G* (GPa)
0.00	0.00	5.012	-	-	0.610 0	159.01(3)	-	-	-	-
1.88	1.71	5.078	0.155 8	0.251 8	0.606 0	156.94(4)	7.78	4.81	150.7	117.5
3.20	3.12	5.122	0.152 8	0.248 0	0.604 3	155.58(5)	7.91	4.87	158.5	121.5
4.28	4.25	5.157	0.150 8	0.245 2	0.603 2	154.54(4)	8.00	4.92	163.6	124.8
5.22	5.22	5.186	0.148 8	0.242 6	0.602 3	153.66(4)	8.10	4.97	169.5	128.1
6.15	6.10	5.215	0.147 4	0.241 0	0.601 0	152.82(4)	8.15	4.99	173.5	129.8
6.81	6.83	5.234	0.146 4	0.239 8	0.600 2	152.25(4)	8.20	5.01	176.8	131.4
7.54	7.64	5.256	0.145 0	0.238 0	0.599 5	151.63(4)	8.27	5.04	181.4	133.5
8.24	8.47	5.276	0.143 8	0.236 6	0.599 1	151.05(4)	8.33	5.06	185.9	135.1
8.88	9.15	5.294	0.142 8	0.235 4	0.598 7	150.54(4)	8.39	5.09	189.7	137.2
9.57	9.75	5.313	0.141 8	0.234 2	0.598 3	149.99(5)	8.44	5.11	193.5	138.7

* Pressures calculated using equation (8) in Whitaker et al. (2008). [b] Pressures measured by NaCl standard. Values in parentheses are 1σ error in the last digits. Two-way travel times have 1σ of ~0.4 ns for S waves (2*ts*) and ~0.2 ns for P waves (2*tp*). The precision of image measurement of sample length is 0.2%–0.4%. Uncertainties in velocities are <0.3%, and <1.0% for the derived elastic moduli. Densities at high pressures are calculated using unit-cell volumes obtained from X-ray data and the theoretical density.

right within the range of those obtained in previous studies (see Table 2). The changes in unit-cell volume with pressure are compared with the results of Merkel et al. (2002) in Fig. 3. Results of third-order Birch-Murnaghan fits (equation (8) in Whitaker et al., 2008) of the *P*-*V* data for these experiments are shown on the diagram. These data agree well with the results of Merkel et al. (2002) within the pressure range explored.

Figure 4a shows the variation of P- and S-wave velocities as a function of pressure, and Fig. 4b shows the change in derived elastic moduli with pressure. The densities and velocities determined experimentally can be fit to third-order finite-strain equations of-state, as shown in Whitaker et al. (2008), to determine elastic properties of the pyrite sample at the reference conditions of 0 GPa and 300 K. By fitting all of the experimental ultrasonic and X-ray data, we obtain the following parameters for FeS_2: K_{S0}=138.9(7) GPa, G_0=112.3(3) GPa, $(\partial K_{S0}/\partial P)_T=K_{S0}'$=6.0(1), $(\partial G_0/\partial P)_T=G_0'$=3.0(<1). Adiabatic results were converted to isothermal values using the following relationship

$$K_S = K_T(1+\alpha\gamma T) = K_T\left(1+\frac{\alpha^2 K_S V T}{C_P}\right) \quad (1)$$

where the thermal expansion coefficient α(300 K)=2.57×10^{-5} K^{-1} (Skinner, 1966), the volume V is the V_0 measured in this experiment (159.01 Å^3), the

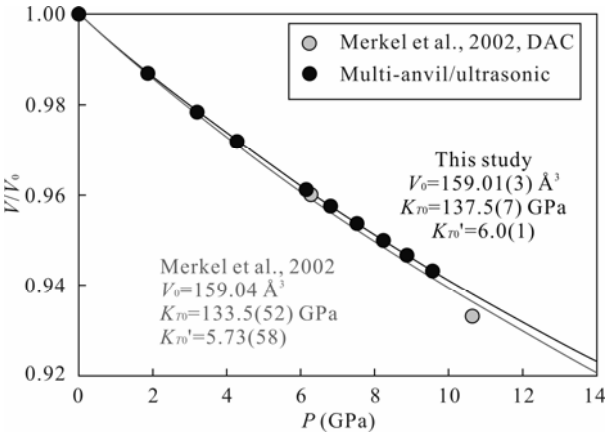

Figure 3. Volume change versus pressure for the ultrasonic experiment on FeS_2. Reference data plotted in background from Merkel et al. (2002). Parameters obtained from third-order Birch-Murnaghan fits are shown for both datasets.

Table 2 Comparison of elastic properties of FeS_2 with previous studies

Ref.	Method	*P* (GPa)	V_0 (Å^3)	K_{S0} (GPa)	K_{S0}'	K_{T0} (GPa)	K_{T0}'	G_0 (GPa)	G_0'
1	Ultrasonics w/X-ray	9.6	159.01(3)	138.9(7)	6.0(1)	137.5	6.0	112.3(3)	3.0(<1)
1	XRD-MAC	9.6	159.01(3)	-	-	137.51(1)	6.01(1)	-	-
2	Linear compression	0.3	-	-	-	148	-	-	-
3	Diffuse X-ray	0	158.34	-	-	147*	-	131	-
4	Ultrasonic	0	158.87	147.9	-	-	-	132.3	-
5	Ultrasonic	0.15	159.05	154.7	7.1	-	-	122.5	2.6
6	XRD	30	-	-	-	148	5.5	-	-
7	XRD-DAC	34	159.04	-	-	215	5.5	-	-
8	XRD-DAC	4.2	158.96	-	-	157	-	-	-
9	Shockwave	180	-	162(9)	-	-	-	-	-
10	XRD-DAC	41.44	159.04	-	-	133.5(52)	5.73(58)	-	-
11	Calculation	Calc. 44 GPa	157.33	157.5	-	154.5	-	-	-
12	Calculation	Calc. 150 GPa	158.87	-	-	176.21	4.65	-	-
13	Calculation	Calc. 135 GPa	159.035	-	-	150	4.56	131	1.85

1. This study; 2. Bridgman (1949); 3. Prasad and Wooster (1956; *from Ref. 2); 4. Simmons and Birch (1963); 5. Benbattouche et al. (1989); 6. Drickamer et al. (1967); 7. Chattopadhyay and von Schnering (1985); 8. Fujii et al. (1986); 9. Ahrens and Jeanloz (1987); 10. Merkel et al. (2002); 11. Sithole et al. (2003); 12. Blanchard et al. (2005); 13. Le Page and Rodgers (2005). MAC. Multi-anvil cell; DAC. diamond anvil cell.

temperature T=300 K, and the heat capacity at constant pressure C_P=62.17 J·mol^{-1}·K^{-1} (Robie et al., 1979), giving K_S/K_T=1.010 6. The pressure derivative of the adiabatic bulk modulus was not converted to isothermal because the difference between the adiabatic and isothermal values for this parameter is expected to be less than the associated uncertainty. A separate third-order Birch-Murnaghan equation of state fitting of the pressure and volume data yields the same result for the bulk modulus (and its pressure derivative) as was obtained via the above conversion relationship (see the second row of data from this study in Table 2). The pressure on the sample was then calculated directly using the third-order Birch-Murnaghan equation of state; these pressures are given in Table 1.

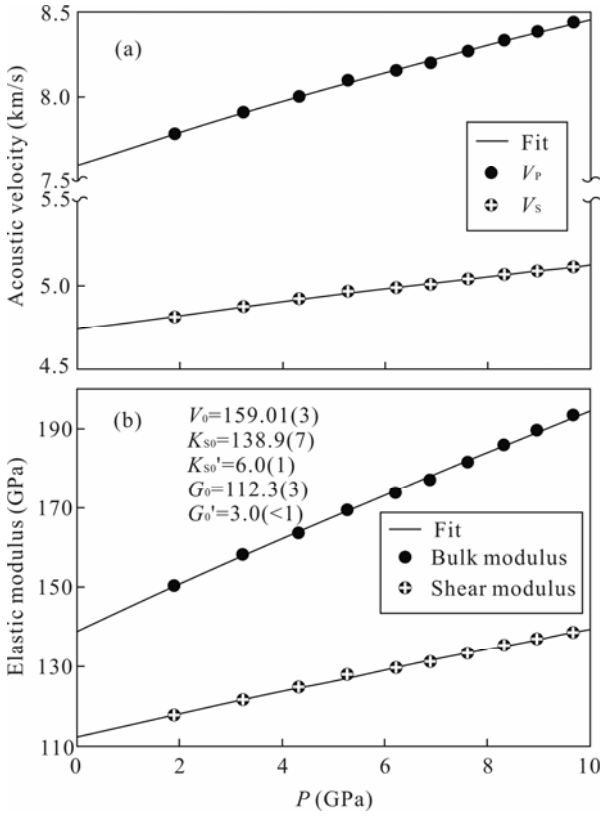

Figure 4. (a) Acoustic velocities in FeS_2 versus pressure. Black circles represent P-wave velocities; circles with crosshairs represent S-wave data. (b) Elastic modulus of FeS_2 versus pressure. Black circles are adiabatic bulk modulus; circles with crosshairs represent shear modulus. Fitting results are shown on (b). The continuous curves are calculated from these fitted parameters.

DISCUSSION

Table 2 presents a comparison of the results of this study with those of previous studies on FeS_2. The V_0 and K_{T0} fall within the range of values from previous experimental investigations (158.34–159.05 Å^3 and 133.5–215 GPa, respectively), while the K_{T0}' obtained here is slightly higher than this range (6.0 versus 5.5–5.73). The bulk modulus obtained from a shockwave study on pyrite (Ahrens and Jeanloz, 1987) is higher than the results obtained by all but one static compression study (162 versus 133–157), even taking into account the adiabatic to isothermal conversion. The results of the study by Chattopadhyay and von Schnering (1985) found a K_{0T} of 215 GPa, which is more than 20% higher than all other experimental and computational results on pyrite (133.5–176 GPa). The results reported here are in very good agreement with the results of Merkel et al. (2002) despite being conducted in a different experimental apparatus.

The elastic bulk and shear modulus and their first pressure derivatives as obtained by first-principles calculations exhibit a marked discrepancy from those obtained experimentally. The K_0 values obtained via these calculations overlap the upper limit of the range found in static experiments and range to higher values (150 to 176 GPa versus 133.5 to 157 GPa), and the K_{0T}' is below the range observed experimentally (4.56 to 4.65 versus 5.5 to 6.0). The G_0 obtained via first principles is the same as the Voigt-Reuss-Hill average (VRH) of single crystal elastic constants from two previous studies (131 GPa, Le Page and Rodgers, 2005; 131 GPa, Prasad and Wooster, 1956; 132.3 GPa, Simmons and Birch, 1963) and higher than that obtained in both this investigation (112.3 GPa) and one previous single-crystal study (122.5 GPa, Benbattouche et al., 1989), while the G_0' obtained via calculations is significantly lower (1.85, Le Page and Rodgers, 2005) than that obtained here (3.0) and from single-crystal data (2.6, Benbattouche et al., 1989) .

It should be noted that much like the trade-off between K_0 and K_0', an increase in G_0 leads to a decrease in G_0' during the fitting process, and vice versa. If the dataset presented here is fit with either G_0 or G_0' fixed to the values presented in Le Page and Rodgers (2005), the fitting results match those presented in that study much more closely, though there is still a dis-

crepancy. These types of discrepancies are commonly seen between experimental results and theoretical calculations, especially in iron minerals, and are caused both by the assumptions that need to be taken in order to conduct these types of calculations, and the fact that such calculations are most commonly conducted at 0 K, while experimental results most commonly have a reference temperature of ~300 K.

The G_0 obtained via the present experiment is lower than those obtained in previous experimental and computational studies (112.3 versus 122.5–132.3). It should be noted that two previous studies on the single-crystal elastic constants of pyrite contain no information on G_0' (Simmons and Birch, 1963; Prasad and Wooster, 1956), while one does have data up to a pressure of 0.15 GPa. The ratio of V_P/V_S obtained in this study (1.60) is very similar to the value of 1.61 obtained by Benbattouche et al., (1989), while the data from other studies give a lower value (1.56, Le Page and Rodgers, 2005; Simmons and Birch, 1963; Prasad and Wooster, 1956) signaling that the shear modulus obtained in these studies may be too high.

The present study fits the data to determine not only the shear modulus and its pressure derivative, but the bulk modulus and its pressure derivative as well, leading to a more complete data set. In addition, the present dataset is not subject to the effects of pressure calibration using a secondary standard; these factors lead to very robust and internally consistent results. It is possible, as mentioned previously, that an increase in G_0' can lead to a decrease in G_0 during the fitting process. While the G_0' determined here (3.0) is quite high compared to many other earth materials (see Hofmeister and Mao, 2003), it is very similar to the value of 2.6 found for pyrite by Benbattouche et al. (1989), as well as that found for ε-FeSi (Whitaker et al., 2009, 2008), which is also a cubic iron mineral.

The discrepancies may have resulted from compositional differences in the single crystal samples used in those studies. None of the samples used in those studies were pure stoichiometric FeS_2 (Benbattouche et al., 1989; Simmons and Birch, 1963; Prasad and Wooster, 1956), unlike the sample used in the present study. In fact, Simmons and Birch (1963) noted that one of their single crystal samples of pyrite had small quartz inclusions, which may have had a significant effect on their results. Pyrite also has high elastic shear anisotropy at ambient conditions according to its single crystal elastic constants. It is possible that some preferred orientation in the polycrystalline aggregate used in this study would therefore lead to a reduced G_0. The destruction of the sample by the blowout during the experiment prevents further assessment of this possibility, but the X-ray diffraction patterns of the sample do not indicate any clearly dominant reflections indicative of preferred orientation.

There may also be some minor effects of deviatoric stress accumulated during compression of the sample. Whitaker et al. (2008) compared the results of measurements made on ε-FeSi at room temperature during cold compression and during decompression after heating and chose the latter dataset as being more accurate because any possible stress effect had been alleviated during heating. However, there were three sources for the discrepancy between the two datasets listed in that study: stress, porosity closure during compression, and differences in pressure range (Whitaker et al., 2008). How much each of these three sources contributed to the overall discrepancy in the data is unknown, but the X-ray diffraction peak widths (FWHM) showed no discernable change during compression, indicating that the differential stress experienced by the sample was minimal (Whitaker et al., 2008).

The X-ray diffraction peaks of pyrite collected in this study also showed no detectable change in their widths during compression, again indicating that the level of deviatoric stress on the sample was quite low. In addition, pressures calculated as discussed earlier match the pressures given by the NaCl pressure standard very closely (see Table 1), which also suggests a low level of differential stress on the sample. The data presented here were collected over a similar pressure range and yielded results similar to those in Whitaker et al. (2008). Conservatively assuming that all of the discrepancy between the two datasets in Whitaker et al. (2008) arises from deviatoric stress on the sample would indicate that the values for the bulk modulus and shear modulus were lowered by 2.4% and 2.8%, respectively, by this stress effect. Assuming that similar deviations can be expected in the pyrite sample

leads to changes in the bulk modulus that are still well within the range of values given by previous studies, and the shear modulus remains below the Reuss bounds given by single crystal elastic constants (Ben-battouche et al., 1989; Simmons and Birch, 1963; Prasad and Wooster, 1956). Similarly, applying the deviations in K_{S0}' and G_0' between the two datasets in Whitaker et al. (2008) to the values obtained here still results in K_{S0}' and G_0' values that are quite high compared to many other earth materials (Hofmeister and Mao, 2003) but very similar to ε-FeSi (Whitaker et al., 2008), which is also a cubic ILEA. Therefore, we feel that the results presented here are very robust despite any effect the presence of minor deviatoric stress may have had on the measurements.

This study presents the first complete high-pressure experimental dataset on the elastic bulk and shear moduli of pyrite and their first pressure derivatives and provides an important benchmark for future studies on this material. To fully investigate the properties of pyrite and to assess the likelihood of sulfur as a possible constituent of the earth's core, the temperature dependence of its physical properties must also be ascertained, which is the focus of an upcoming experimental investigation. The results presented here provide some important new insights into the pyrite form of FeS_2 and provide some new constraints for refining models and calculations involving FeS_2 and its physical properties under extreme conditions by making available the first data on the shear modulus of this phase and its first pressure derivative.

ACKNOWLEDGMENTS

The authors gratefully acknowledge the constructive reviews of two anonymous reviewers which helped to improve this manuscript. We also thank T Irifune, J F Zhang, and L Dobrzhinetskaya for organizing and editing this special issue. This study was supported by the USA National Science Foundation (Nos. EAR00135550, EAR0635860) to Baosheng Li, the USA Department of Energy, Office of Science, Office of Basic Energy Sciences (No. DE-AC02-98CH10886), the Consortium for Materials Properties Research in Earth Sciences under NSF Cooperative Agreement (No. EAR01-35554), and the Mineral Physics Institute, Stony Brook University (MPI Publication No. 480).

REFERENCES CITED

Ahrens, T. J., Jeanloz, R., 1987. Pyrite-Shock Compression, Isentropic Release, and Composition of the Earth's Core. *Journal of Geophysical Research*, 92(B10): 10363–10375

Badro, J., Fiquet, G., Guyot, F., et al., 2007. Effect of Light Elements on the Sound Velocities in Solid Iron: Implications for the Composition of Earth's Core. *Earth and Planetary Science Letters*, 254(1–2): 233–238

Benbattouche, N., Saunders, G. A., Lambson, E. F., et al., 1989. The Dependences of the Elastic Stiffness Moduli and the Poisson Ratio of Natural Iron Pyrites FeS_2 upon Pressure and Temperature. *Journal of Physics D*: *Applied Physics*, 22(5): 670–675

Blanchard, M., Alfredsson, M., Brodholt, J., et al., 2005. Electronic Structure Study of the High-Pressure Vibrational Spectrum of FeS_2 Pyrite. *Journal of Physical Chemistry B*, 109(46): 22067–22073

Bridgman, P. W., 1949. Linear Compressions to 30 000 kg/cm^2, Including Relatively Incompressible Substances. *Proceedings of the American Academy of Arts and Sciences*, 77(6): 189–234

Chattopadhyay, T., von Schnering, H. G., 1985. High Pressure X-Ray Diffraction Study on P-FeS_2, M-FeS_2 and MnS_2 to 340 kbar: A Possible High Spin-Low Spin Transition in MnS_2. *Journal of Physics and Chemistry of Solids*, 46(1): 113–116

Chrystall, R. S. B., 1965. Thermal Expansion of Iron Pyrites. *Transactions of the Faraday Society*, 61(512P): 1811

Dreibus, G., Palme, H., 1996. Cosmochemical Constraints on the Sulfur Content in the Earth's Core. *Geochimica et Cosmochimica Acta*, 60(7): 1125–1130

Drickamer, H. G., Lynch, R. W., Clendenen, R. L., et al., 1967. X-Ray Diffraction Studies of the Lattice Parameters of Solids under very High Pressure. *Solid State Physics*, 19: 135–228

Dziewonski, A. M., Anderson, D. L., 1981. Preliminary Reference Earth Model. *Physics of the Earth and Planetary Interiors*, 25(4): 297–356

Fujii, T., Yoshida, A., Tanaka, K., et al., 1986. High Pressure Compressibilities of Pyrite and Cattierite. *Mineralogical Journal*, 13(4): 202–211

Hofmeister, A. M., Mao, H. K., 2003. Pressure Derivatives of Shear and Bulk Moduli from the Thermal Gruneisen Parameter and Volume-Pressure Data. *Geochimica et Cos-*

mochimica Acta, 67(6): 1207–1227

Jeanloz, R., 1990. The Nature of the Earth's Core. *Annual Review of Earth and Planetary Sciences*, 18: 357–386

Jephcoat, A., Olson, P., 1987. Is the Inner Core of the Earth Pure Iron. *Nature*, 325(6102): 332–335

Kleppe, A P.. K., Jephcoat, A. P., 2004. High-Pressure Raman Spectroscopic Studies of FeS_2 Pyrite. *Mineralogical Magazine*, 68(3): 433–441

Le Page, Y., Rodgers, J. R., 2005. Ab Initio Elasticity of FeS_2 Pyrite from 0 to 135 GPa. *Physics and Chemistry of Minerals*, 32(8–9): 564–567

Li, B. S., Chen, K., Kung, J., et al., 2002. Sound Velocity Measurement Using Transfer Function Method. *Journal of Physics—Condensed Matter*, 14(44): 11337–11342

Li, B. S., Kung, J., Liebermann, R. C., 2004. Modern Techniques in Measuring Elasticity of Earth Materials at High Pressure and High Temperature Using Ultrasonic Interferometry in Conjunction with Synchrotron X-Radiation in Multi-anvil Apparatus. *Physics of the Earth and Planetary Interiors*, 143–144: 559–574

Li, J., Agee, C. B., 2001. Element Partitioning Constraints on the Light Element Composition of the Earth's Core. *Geophysical Research Letters*, 28(1): 81–84

Li, J., Fei, Y., Mao, H. K., et al., 2001. Sulfur in the Earth's Inner Core. *Earth and Planetary Science Letters*, 193(3–4): 509–514

Mao, H. K., Shu, J. F., Shen, G. Y., et al., 1998. Elasticity and Rheology of Iron above 220 GPa and the Nature of the Earth's Inner Core. *Nature*, 396(6713): 741–743

McDonough, W. F., Sun, S. S., 1995. The Composition of the Earth. *Chemical Geology*, 120(3–4): 223–253

Merkel, S., Jephcoat, A. P., Shu, J., et al., 2002. Equation of State, Elasticity, and Shear Strength of Pyrite under High Pressure. *Physics and Chemistry of Minerals*, 29(1): 1–9

Oldham, R. D., 1906. The Constitution of the Interior of the Earth, as Revealed by Earthquakes. *Quarterly Journal of the Geological Society*, 62(1–4): 456–475

Prasad, S. C., Wooster, W. A., 1956. The Elasticity of Iron Pyrites, FeS_2. *Acta Crystallographica*, 9(2): 169–173

Robie, R. A., Hemingway, B. S., Fisher, J. R., 1979. Thermodynamic Properties of Minerals ad Related Substances at 298.15 K and 1 bar (10^5 Pascals) Pressure and at Higher Temperatures. *United States Geological Survey Bulletin*, 1452: 298–310

Simmons, G., Birch, F., 1963. Elastic Constants of Pyrite. *Journal of Applied Physics*, 34(9): 2736–2738

Sithole, H. M., Ngoepe, P. E., Wright, K., 2003. Atomistic Simulation of the Structure and Elastic Properties of Pyrite (FeS_2) as a Function of Pressure. *Physics and Chemistry of Minerals*, 30(10): 615–619

Skinner, B. J., 1966. Thermal Expansion. In: Clark, S. P. J., ed., Handbook of Physical Constants. Geological Society of America, Boulder, CO. 75–95

Smith, F. G., 1942. Variation in the Properties of Pyrite. *American Mineralogist*, 27(1): 1–19

Whitaker, M. L., Liu, W., Liu, Q., et al., 2008. Combined In Situ Synchrotron X-Ray Diffraction and Ultrasonic Interferometry Study of Epsilon-FeSi at High Pressure. *High Pressure Research*, 28(3): 385–395

Whitaker, M. L., Liu, W., Liu, Q., et al., 2009. Thermoelasticity of Epsilon-FeSi to 8 GPa and 1 273 K. *American Mineralogist*, 94(7): 1039–1044